multi-Risk sciEnce for resilienT commUnities undeR a changiNg climate

Codice progetto MUR: **PE00000005** – **I33C22006910006**

Deliverable title: Paleo and historical climate datasets for Italian regions.

Deliverable ID: 8.2.2

Due date: 30 November 2024

Submission date: 27 February 2025

AUTHORS

Marco Borga (UNIPD); Marco Marani (UNIPD); Eleonora Dallan (UNIPD); Alberto Montanari (Unibo); Mattia Neri (UNIBO); Rui Guo (UNIBO); Serena Ceola (UNIBO)

1. Technical references

Project Acronym	RETURN
Project Title	multi-Risk sciEnce for resilienT commUnities undeR a changiNg climate
Project Coordinator	Domenico Calcaterra UNIVERSITA DEGLI STUDI DI NAPOLI FEDERICO II domcalca@unina.it
Project Duration	December 2022 – November 2025 (36 months)

Deliverable No.	DV8.2.2
Dissemination level*	CO
Work Package	WP2 - – State of the art and knowledge base to define impact-oriented hazard indicators
Task	T8.2.2 - Collection, harmonisation and analysis of paleo and historical climate records.
Lead beneficiary	UNIPD
Contributing beneficiary/ies	UNIBO

PU = Public

PP = Restricted to other programme participants (including the Commission Services)

RE = Restricted to a group specified by the consortium (including the Commission Services)

* CO = Confidential, only for members of the consortium (including the Commission Services)

Document history

Version	Date	Lead contributor	Description
0.1	18.11.2024	Alberto Montanari (UNIBO)	First draft
0.2	25.02.2025	Marco Borga and Marco Marani (UNIPD)	Critical review and proofreading
1.0	27.02.2025	Alberto Montanari (UNIBO)	Final version

2. ABSTRACT

This document describes the setup of an innovative procedure to reconstruct paleoclimatic river flows. Paleo-climatic data are essential to assess flood and drought risk, with uncertainty assessment, therefore overcoming the problem of the limited sample size of historical records.

The procedure herein proposed can be applied to any large catchment of Italy and Europe. It emulates analogous experiments carried out for the American continent. It is applied for the first time in Italy. The results demonstrate the excellent capabilities of the proposed method to capture the historical variability of river flow for the relevant case of the Po River.

The procedure is described here by including a copy of a paper that has been just accepted for publication in an international prestigious journal.

3. Table of contents

Bridging information from paleo-hydrological and climate model ensembles to assess long term hydrological drought hazard

Rui Guo[1], Hung T. T. Nguyen[2], Stefano Galelli[3], Serena Ceola[1], Alberto Montanari[1]

[1]Department of Civil, Chemical, Environmental, and Materials Engineering (DICAM), Alma Mater Studiorum Università di Bologna, Bologna, Italy
[2]Department of Earth Science and Environmental Change, University of Illinois Urbana-Champaign, Illinois, USA
[3]School of Civil and Environmental Engineering, Cornell University, Ithaca, New York, USA

Key Points:

- Framework for drought hazard estimation through river flow observations, tree-ring-based reconstructions, and climate model simulations
- Millennium-long evolution of multiyear hydrological drought features in Alpine regions under anthropogenic global warming
- Unprecedented drought conditions may occur in Alpine regions in the coming decades compared to the past nine centuries

Corresponding author: Rui Guo, `rui.guo2@unibo.it`

Abstract

Characterizing the evolution of drought frequency and severity under anthropogenic global warming remains a key challenge because of the mismatch between the length of instrumental records and the long-term variability of drought features. To address this gap, we propose a modeling framework that combines river flow observations, paleo-hydrological reconstructions, and climate model simulations. Such diversity of climate information, that is bridged in a flexible approach, allows evaluating the hazard of hydrological droughts for any large catchment globally. By focusing on the specific case of Alpine regions and analyzing the information contained in an ensemble for the period 1100–2100, we show that, compared to the past nine centuries, the mean annual flow in the Po River (Italy's main water course) may decrease by about 10% during the 21st century, while the mean drought duration and severity are likely to increase by approximately 11% and 12%, respectively. Future drought conditions are likely to match, or even exceed, the driest period of the Medieval Climate Anomaly under different emissions scenarios. This indicates unprecedented drought conditions in Alpine regions in the coming decades, thus calling for an increased preparedness in managing water resources under climate change.

Plain Language Summary

The frequent occurrence of droughts, particularly hydrological droughts, has raised the concern that future climate changes may lead to increasing drought hazards which strongly impacts different socio-economical sectors. Predicting the evolution of hydrological drought features remains a key challenge due to the length of observational data generally insufficient to infer the long-term variability of these processes. We propose to address the problem through an approach that can be applied to any large river basin globallyand that is based on the integration of in-situ river flow observations, tree-ring-based river flow reconstruction, and climate model simulations. For the specific case of Alpine regions, we obtain a flexible set of long term climatic information to frame contemporary and future droughts into a millennium-long hydroclimatic background and evaluate whether these events are precursors of increasing drought hazard. Our finding indicates that unprecedented drought conditions may occur in Alpine areas in the coming decades, suggesting the region needs to increase its preparedness in managing water resources under climate change.

1 Introduction

Major droughts occurring with increasing frequency have raised the concern that future changes in climate may lead to an increase in drought hazard (Ault, 2020). The worsening of hydrological droughts is of particular concern, as water availability in rivers and other water bodies strongly impacts agriculture, energy production, socio-economical assets, and, ultimately, public health (Van Loon & Laaha, 2015; Stahl et al., 2016; Ukkola et al., 2020). The concern is particularly relevant in Alpine regions where the seasonality of river flows is changing under global warming (Montanari et al., 2023). In addition to climatic drivers, anthropogenic activities such as urbanization, irrigation, and dam operations may also profoundly reshape hydrological drought dynamics, by exacerbating or alleviating the frequency, duration, and severity of droughts (AghaKouchak et al., 2015; Van Loon, Gleeson, et al., 2016; Van Loon, Stahl, et al., 2016; Di Baldassarre et al., 2018; AghaKouchak et al., 2021). Unlike other extreme events, droughts may persist for several years, thus resulting in "multiyear droughts" (Van Dijk et al., 2013; Sousa et al., 2018; Lund et al., 2018), with 5–10 years duration, and "megadroughts", with duration even longer than a decade (B. I. Cook et al., 2016, 2022). These events cause profound impacts on water systems and socio-economic settings.

Predicting the evolution in the frequency and severity of hydrological droughts remains a key challenge because of the mismatch between the length of the available observational data and the decadal and multi-decadal timescales that characterize the long-term variability of these processes (Ault et al., 2013, 2014; B. I. Cook et al., 2015). While only a few rainfall and river flow records span more than 200 years (Marani & Zanetti, 2015; Montanari et al., 2023), most span only a few decades (Galelli et al., 2021), which is insufficient to infer the dynamics of severe hydrological droughts. Moreover, anthropogenic global warming adds additional uncertainty as historical statistics may not be fully representative of future conditions.

A number of studies showed that paleo-reconstructions of hydroclimatic variables based on proxy data (e.g., tree-rings) provide valuable insights of natural variability during the pre-instrumental period (Büntgen et al., 2011; Rao et al., 2020; B. I. Cook et al., 2022; Khan et al., 2022; Chen et al., 2023). In particular, drought atlases—tree-ring-based paleoclimate reconstructions of the self-calibrating Palmer Drought Severity Index (scPDSI, (Wells et al., 2004))—have been used as reliable proxies for river flow reconstruction over North America (Ho et al., 2016, 2017) and Asia (Nguyen & Galelli, 2018; Nguyen et al., 2020; Wu et al., 2022). While proxy-based reconstructions undoubtedly play a pivotal role in unraveling statistical properties of past climate, they are, alone, insufficient to provide a comprehensive understanding of the underlying physical processes governing changes in the climate system. General circulation models (GCMs) fill this gap by simulating the physical climate processes and providing a suite of climate variables that represent climate dynamics at different spatial and temporal scales in a way that proxies cannot (PAGES Hydro2k Consortium, 2017). Specifically, model outputs from phase six of the Coupled Model Intercomparison Project (CMIP6) (O'Neill et al., 2016) and phase four of the Paleoclimate Model Intercomparison Project (PMIP4) (Kageyama et al., 2018) include simulations of runoff (i.e., river flow per unit area) covering the period 850–2100, which can be used to estimate river flow. By combining these climate simulations with paleo-hydrological reconstructions and historical observations, one can derive ensembles that provide a detailed quantitative characterization of past, present, and future hydrological droughts (E. R. Cook, Seager, et al., 2010; B. I. Cook et al., 2015; PAGES Hydro2k Consortium, 2017; Hessl et al., 2018), while considering inherent uncertainties and limitations. Here, we propose a framework for integrating the above information through cross-validation procedures to test their mutual agreement in the reconstruction of drought features. The diversity of the underlying information allows the application of the framework to any large river catchment with the capability to adapt to different situations of data availability.

In particular, we show that the information contained in the above ensembles reveals key features about the evolution of future drought hazards in the Po River basin (Italy) , which is the collector of the main water courses of the Alpine regions of Northern Italy. By integrating in-situ river flow observations, tree-ring-based river flow reconstructions, and PMIP4 and CMIP6 simulations, we frame contemporary drought events into a millennium-long hydroclimatic background (1100–2100) and evaluate whether these events are precursors of increasing drought hazard (IPCC, 2021; Essa et al., 2023). The choice of this case study is driven by the socio-economic importance of the basin, which supports around 40% of Italy's gross domestic product, supplies 35% of the food demand, and generates 45% of the total hydropower over the country (Autorità di Bacino del Fiume Po, 2006). Perhaps more importantly, 6 out of the 10 worst droughts reported in instrumental records of the Po River flow occurred after 2000 (Montanari et al., 2023), with the last one peaking in 2022 and causing the worst hydrological drought in the past two centuries (Montanari et al., 2023; Avanzi et al., 2024). Being able to characterize the evolution of drought characteristics is therefore key to support water resources management under changing climatic conditions.

2 Materials and Methods

To introduce the proposed framework for hydrological drought hazard assessment we focus here on the case of the Po River. Our framework combines the information from long term river flow observations, paleo-river flow reconstructions and global climate models.

2.1 River flow observations

Since the beginning of the 19th century, river stages (i.e., water levels) in multiple locations along the Po River have been regularly measured (Zanchettin, Traverso, & Tomasino, 2008). In particular, the river stage at Pontelagoscuro, which is considered the closure of the more than 70,000 km^2 Po River basin, has been monitored since 1807. The monthly flow of the Po River from 1807 to 1916 has been reconstructed by using the rating curve at Pontelagoscuro (Zanchettin, Traverso, & Tomasino, 2008), which was estimated in the 1920s by the National Hydrographic Service of Italy (Giovannelli & Allodi, 1960; Montanari, 2012). By merging the above reconstruction with modern instrumental data, a monthly record spanning from 1807 to the present day was obtained and applied in several studies with comparative assessments that validate the robustness of the time series (Zanchettin, Rubino, et al., 2008; Taricco et al., 2015; Rubinetti et al., 2020; Montanari et al., 2023). We use this 217-year record (from Jan 1, 1807 to Dec 31, 2023)—at annual time scale—as the in-situ observation to benchmark the mean annual river flow reconstruction and the GCM simulations (Fig. S1).

2.2 Old World Drought Atlas as proxy data for river flow reconstruction

For paleo-climate proxy data, we use the Old World Drought Atlas (OWDA) (E. R. Cook et al., 2015), a gridded dataset of the self-calibrating Palmer Drought Severity Index (scPDSI, (Wells et al., 2004)). The OWDA was reconstructed from 106 tree-ring chronologies and has a spatial resolution of $0.5° \times 0.5°$, spanning Europe, North Africa and the Middle East. Each grid cell represents a time series of mean June-July-August (JJA) scPDSI from 0–2012. Drought atlases reconstructed from tree-rings provide a physical and statistical basis for river flow reconstruction (Ho et al., 2016; Nguyen et al., 2020). Since both river flow and scPDSI can be modeled as functions of ring width, one can build a model to relate river flow to scPDSI directly. Unlike tree-rings, which are generally irregular in space and time, drought atlases provide a more consistent and homogenous gridded dataset, analogous to converting distributed climate station data into a unified gridded climate data, thereby simplifying the application of our framework without the need for detrending, standardizing, or nesting as required for tree-rings chronologies (Nguyen et al., 2020). Although uncertainty exists in drought atlases (since they are regression products based on tree-ring data), the computational advantages of using drought atlases make the framework easy to reuse and suitable for both small- (Coulthard et al., 2016; Nguyen & Galelli, 2018) and large-scale reconstructions (Ho et al., 2017; Nguyen et al., 2020; Wu et al., 2022). Here, we use the OWDA portion between 1100—2012 to reconstruct annual river flow, as this is the stable portion with a sufficient number of tree-ring chronologies in the source tree-ring network (Fig. S2).

2.2.1 Climate-informed proxy selection, reconstruction, and cross-validation

A proper selection of tree-ring sequences is necessary to filter noise and retain only OWDA grid cells with a positive correlation with the observed river flow. To maintain both geographical proximity and hydroclimatic similarity between the river gauging station and an OWDA grid cell, we follow the hydroclimate characterization of Knoben et al. (2018) with a search radius. Accordingly, the hydroclimate at a location is characterized by three indices: aridity (a), moisture seasonality (s), and snow fraction (f) for a global 0.5°×0.5° resolution. The hydroclimatic similarity between two locations i and j is defined as their Euclidean distance in the hydroclimate space. We label this distance as d_{KWF}, which is given by:

$$d_{KWF}(i,j) = \sqrt{(a_i - a_j)^2 + (s_i - s_j)^2 + (f_i - f_j)^2}. \quad (1)$$

By calculating d_{KWF} between each OWDA grid point and the river gauging station, we can screen out OWDA grid points that are geographically close to the station but hydroclimatically different. We vary the d_{KWF} between 0.1 and 0.3 in 0.05 increments. For each value of d_{KWF} we screen grid points within a radius of 1,200 km encompassing a set of the OWDA grid points surrounding the river gauging station. In our search regions for the Po River, scPDSI often correlates significantly and positively with river flow and the correlation pattern generally retains across distinct time windows (Fig. S3-S4).

Next, we perform a weighted principal component analysis (PCA) to remove multicollinearity among the OWDA grid points. Following the Point-by-Point Regression (PPR) method (E. R. Cook & Kairiukstis, 2013), we weight each grid point by its correlation with the observed river flow, by using the relationship

$$z_i = g_i \cdot {r_i}^p. \quad (2)$$

Here, g_i is the scPDSI time series at grid point i, r_i is the correlation between g_i and the observed river flow, p is the weight exponent, and z_i is the weighted version of g_i. We use p values equal to 0, 0.5, 2/3, 1, 1.5 and 2, as in E. R. Cook, Anchukaitis, et al. (2010). We then perform PCA on the obtained z_i time series and retain only those principal components (PCs) with eigenvalues $\geq$ 1.0 (Hidalgo et al., 2000). For each combination of d_{KWF} and PCA weight p, we select a parsimonious subset from the retained PCs that is most relevant to the observed river flow by using the VSURF (Variable Selection Using Random Forest) algorithm (Genuer et al., 2010). Therefore, we end up with an ensemble of 30 such subsets, the best of which is further selected using cross-validation and adopted for the final reconstruction.

Finally, we build linear regression models between all the subsets of PCs and observed annual river flow. The reconstruction algorithm is implemented in the R package "ldsr" (Nguyen et al., 2020). We choose the 93-year window 1920–2012 as the calibration-validation period, during which daily and quality-checked river flow data are available. To capture regime shift and retain enough data points for calibration, we used a leave-20%-out cross-validation scheme. In each cross-validation run, we withhold a contiguous chunk of 20% of the data points for validation, and train the model on the remaining 80% record. Cross-validation is repeated 30 times to obtain the ensemble reconstruction and get distributions of skill scores, which yield a reasonably robust mean estimate for each metric. Four goodness-of-fit statistics, i.e., (1) Coefficient of Determination (R^2), (2) Nash-Sutcliffe Coefficient of Efficiency (NSE, (Nash & Sutcliffe, 1970)), (3) Kling-Gupta Efficiency (KGE, (Gupta et al., 2009)), and (4) Normalized Root Mean Squared Error (NRMSE) are computed. After cross-validating all subsets, the final reconstruction for annual river flow of the Po River from 1100 to 2012 is built by selecting the ensemble member with the lowest Euclidean distance between the couple of values (NSE, KGE) and the point (1, 1). Prediction intervals for the reconstructed annual flow is computed by assuming that prediction errors follow a Gaussian probability distribution with the same variance as the residuals of the linear regression.

2.3 Climate model simulations

We obtain the annual runoff (i.e., river flow per unit area) output in the spatial domain of the Po River basin from a 25-GCM-model ensemble of phase six of the Coupled

Model Intercomparison Project (CMIP6) (O'Neill et al., 2016). CMIP6 simulations are available for both historical (1850–2014) and future (2015–2100) periods. Future projections are obtained under the emission scenarios "Shared Socioeconomic Pathway" (SSP) 1-2.6 (SSP1-2.6) and 5-8.5 (SSP5-8.5). These are the scenarios considered by the Scenario Model Intercomparison Project (ScenarioMIP) (O'Neill et al., 2016) of CMIP6. Four of these GCM models also provide the ensemble simulation in the *past1000* and *past2k* experiments (Jungclaus et al., 2017) from phase four of the Paleoclimate Model Intercomparison Project (PMIP4) (Kageyama et al., 2018). The PMIP4 experiments span the time window 850–1849, while the CMIP6 experiments cover the period 1850–2100, so they can be concatenated for these 4 GCMs for PMIP4. Table S1 shows detailed information for the whole set of considered GCMs. Therefore, we obtain both the CMIP6 and the PMIP4 suites, spanning from 1850 to 2100 and 1100 to 2100, respectively. When computing the average annual runoff in the Po River basin using the CMIP6 and PMIP4 ensembles, we bi-linearly interpolate all the runoff data into a common $0.25^\circ \times 0.25^\circ$ grid and then calculate the arithmetic mean value of the grids within the watershed. The sensitivity of the results to regridding is checked by comparing 0.25-degree with 1.5-degree outputs of GCMs (see Fig. S5). The multimodel ensemble mean is the arithmetic average value of the outputs from the CMIP6 and the PMIP4 model ensembles.

2.4 Bias correction

Runoff simulations provided by GCM are at the grid scale. To compare them with observed river flows, one should take into account the potential bias. Therefore, we apply quantile delta mapping (QDM) (Cannon et al., 2015) to correct bias with respect to the observed annual river flow series. QDM preserves model-projected relative change in quantiles, while at the same time correcting the systematic biases in quantiles of a model simulation compared to observed values. QDM has been widely adopted for bias correction of GCM output such as precipitation (Li et al., 2022; Potter et al., 2023). Here, we apply QDM to CMIP6 and PMIP4 model runs and to the reconstructed river flow series to ensure that the historical portion (1850–2012) of the bias corrected records has a similar probability distribution of the observed series while preserving past relative change in quantiles.

2.5 Multiyear drought identification

To cross-validate the reliability of both reconstruction and GCMs in simulating multiyear hydrological droughts, we apply run theory (Yevjevich, 1967) to annual river flow series to characterize drought events in terms of drought frequency (DF), duration (DD), severity (DS), and intensity (DI), as in Guo and Montanari (2023). In detail, the long-term mean river flow R_{LT} is adopted as a reference value to identify positive or negative runs. If river flow in a given year is lower than an assigned threshold T_{lower} (where $T_{lower} < R_{LT}$), a negative run is started; the run ends in the year when the river flow is higher than R_{LT}. If the interval between two negative runs is only one year and river flow in that year is less than a selected upper threshold T_{upper} (where $T_{upper} > R_{LT}$), then these two runs are combined into one drought. Finally, only runs that have a duration of no less than 3 years are labeled as multiyear drought events. We first standardize all the time series to zero mean and unit variance to ensure the drought characteristics can be compared between river flow observations, reconstructions, and GCM simulations. Here, the thresholds T_{upper} and T_{lower} are defined as 0.2 more and 0.25 less than R_{LT}, respectively. These thresholds are identified with a trial and error procedure by verifying that relevant droughts observed in the past are consistently recognised. After identifying a multiyear drought, DD, DS, DI and DF are computed as follows. DD is the time lapse between the start and the end of the event. DS is calculated as the cumulative river flow deficit with respect to R_{LT} during the drought duration divided by the mean river flow. DI is the ratio between drought severity DS and duration DD. DF is estimated by dividing the total number of droughts by the number of years included in the considered observation period.

2.6 Goodness-of-fit testing and cross-validation of GCM simulations

To assess the performance of each of the considered GCMs in reproducing the statistics of annual river flow during the historical period (1850-2012), we use the “Combined Probability-Probability” (CPP) plot (Koutsoyiannis & Montanari, 2022). The two-sample Kolmogorov-Smirnov test (Massey Jr, 1951) is used to quantify the distance between the probability distribution of annual river flows simulated by each GCM and the observed data. We use the Gaussian kernel density estimation (Terrell & Scott, 1992) method to estimate the probability density function of each series.

3 Results

3.1 Cross-validation of tree-ring-based annual flow reconstruction and climate model simulations during 1920–2012

Bias-corrected annual river flow reconstruction and climate model simulations satisfactorily reproduce the observed annual river flow during the period 1920–2012 (Fig. 1). The correlation, bias, and variability of annual data are well captured by the reconstruction model (Coefficient of Determination, R^2=0.52; Nash-Sutcliffe Coefficient of Efficiency, NSE=0.35; Kling-Gupta Efficiency, KGE=0.55; Normalized Root Mean Squared Error, NRMSE=0.02). Note that these results are not sensitive to the grid size of the GCM regridding (Fig. S5).

The long-term mean river flow and multiyear drought events during 1920–2012 (Fig. 1A), including drought frequency, mean duration, mean severity, and mean intensity (Table S2), are well captured by the reconstruction. The mean river flow from the whole reconstruction period (1100–2012) is 1,508 m^3/s, which is only slightly larger than the mean observed river flow during 1807–2012 (1,506 m^3/s). The probability density distributions of reconstructed and GCM simulated annual river flows match the distribution from observed data (Fig. 1B), ensuring reliability for subsequent analyses of the Po River flow regime. For GCM, this result confirms the effectiveness of bias correction—performed with observation spanning from 1850 to 2012—in adjusting the distribution of data.

For GCM simulations, the Combined Probability-Probability (CPP) plot (Koutsoyiannis & Montanari, 2022) and the two-sample Kolmogorov-Smirnov test confirm that one cannot reject the hypothesis that distributions from the models and observations are not different ($p \geq 0.05$, see Fig. S6). Overall, the reliability of the reconstruction and GCM simulations in the historical period allows us to further investigate river flow and hydrological drought changes in a broader hydro-climatological context.

3.2 Cross-validation of paleo and future river regime basing on previous studies, tree-ring-based reconstruction and climate models

From the reconstruction based on tree-rings, we apply run theory to the 30-year moving average series to identify dry periods (see Fig. 2 and Materials and Methods). In general, the results are consistent with previous studies (E. R. Cook et al., 2015; Büntgen et al., 2021; Helama et al., 2009). The Po River experienced several dry periods during the late Medieval Climate Anomaly (MCA) (∼1100–1170, ∼1200–1250), Renaissance (∼1400–1450, ∼1480–1580), and late Little Ice Age (LIA, ∼1750–1810). In addition, the reconstruction replicates documented flood-rich periods (blue shades in Fig. 2A) (Blöschl et al., 2020).

The PMIP4 ensemble exhibits wet (e.g., around the 1300s, ∼1590–1630, ∼1820–1850, and ∼1890–1930) and dry (e.g., 1200–1240, ∼1550–1580, and ∼1750–1790) periods that are consistent with the reconstruction from tree-ring data. Note that our analysis does not provide an indication of the drivers of these periods—i.e., whether they are a result of internal ocean-atmosphere variability or external forcings such as volcanic or solar activity. The PMIP4 ensemble mean, although well simulating the long-term mean river flow (1,502 m^3/s), underestimates the magnitude of multi-decadal hydrological variability.

For the period 2015–2100, both CMIP6 and PMIP4 ensembles consistently project a declining trend in river flow under the SSP5-8.5 scenario (Fig. 2A). By the end of this century, river flow may be as low as that of the driest period in the paleo-climate record (i.e., late MCA). Even under the SSP1-2.6 scenario (Fig. S7), dry conditions similar to that of the late MCA period may occur, although the decrease in mean river flow is not as significant as with SSP5-8.5. The probability density functions of the CMIP6 ensemble, PMIP4 ensemble, reconstruction, and observations for the different periods clearly indicate that the mean annual river flow will decrease by about 10% by 2100 with respect to the corresponding past value (1100–2014) (Fig. 2B), thus suggesting the possibility of extremely dry conditions in terms of mean annual river flow occurring by the end of the 21st century.

3.3 Characteristics of past and future hydrological droughts

We explore the changes of multiyear hydrological droughts in terms of frequency (DF), mean duration (DD), mean severity (DS), and mean intensity (DI, the ratio between DS and DD) during the period 1100–2100 (Fig. 3 and Table S3). River flow reconstruction, CMIP6 and PMIP4 simulations satisfactorily replicate DF, DD, DS and DI during the historical period 1850–2012 with a slight overestimation of DF by the reconstruction and slightly higher DS and DI by CMIP6 (Fig. 3A). Both the reconstruction and PMIP4 depict higher DF and lower DD, DS, and DI in the historical period compared to the pre-historical window (1100–1850). This means that droughts in the Po River were longer and more severe in the distant past than in the last 170 years. This finding is consistent with a previous study (Ionita et al., 2021), which shows that past megadroughts in Europe were longer and more severe than recent droughts.

For future projections (Fig. 3A), CMIP6 shows that the dynamics of hydrological droughts exhibit an increase in both DD and DS under SSP5-8.5 by approximately 11% and 12%, respectively, whereas negligible changes are observed under SSP1-2.6. PMIP4 projections depict an even drier future in terms of DD, DS and DI, with magnitude consistently higher under SSP5-8.5 with respect to SSP1-2.6. Overall, both PMIP4 and CMIP6 indicate that mean DD, DS, and DI of multiyear droughts are projected to reach (under SSP1-2.6) or even surpass (under SSP5-8.5) pre-historical levels.

In fact, the right tails of the probability density functions for DD, DS, and DI (Fig. 3B) suggest possible recurrences of persistent and severe megadroughts under both future emission scenarios, similar to, or even worse than, those identified from river flow reconstruction and PMIP4 simulations, yet unobserved in the historical period. This result is consistent with recent findings that the whole Mediterranean region may face a higher drought hazard in the future (Essa et al., 2023). The picture for drought frequency is different, as a decrease is projected by both PMIP4 and CMIP6 for both emission scenarios with respect to the historical period, with a lower frequency predicted by CMIP6 under SSP5-8.5 with respect to SSP1-2.6. Overall, these outcomes suggest that during the 21st century, we may expect fewer hydrological droughts, but each of them may be longer, more severe, and more intense, with a significant decline of mean annual river flow.

3.4 Placing recent droughts into a broader hydro-climatological context

We compare the features of the above historical extreme events with those of the 2022 hydrological drought that hit the Po River basin. In terms of annual average river flow (based on tree-rings-reconstruction), 2022 emerges as an unprecedented minimum in the past 900 years (Fig. 4A), even if one compares it with the lower bound of the 95% prediction interval. According to PMIP4, a single drought, occurring in late MCA, appeared more intense than the 2022 event (Fig. 4B). However, from the 10-year (Fig. 4C) and 30-year (Fig. 4D) moving averages of annual river flow, both reconstruction and PMIP4 simulations display several past events in which multiyear average flows were lower than the recent period. In fact, by looking at the whole temporal extension of the 2022 drought, which lasted from 2015 to 2023, we confirm that such a multiyear event is unprecedented in the past 200 years, while longer drought events with higher cumulative deficit occurred during MCA and LIA (Fig. 4E). In the coming decades, climate model ensembles under SSP5-8.5 indicate the possible occurrence of more prolonged and exacerbated multiyear droughts than the 2022 one, which may even exceed the worst event during MCA (Fig. 4F). Even under the SSP1-2.6 scenario (Fig. S8), future droughts are likely to occur with similar behaviours as those during MCA from annual to multidecadal scale.

4 Discussion and Conclusions

Through multiple cross-validation we demonstrate that tree-ring-based river flow reconstruction for the past nine centuries of Po River outlet shows a general agreement with GCM-based simulations of paleo-runoff for annual river flows. This includes both dry and flood-rich periods. In addition, both reconstruction and GCM-based simulations are capable of reproducing multiyear drought events during the instrumental period. By assuming that the reliability of such reconstruction and simulations is conserved along the whole period covered by GCMs and paleo-hydrological data, we can study the evolution of drought characteristics throughout the millennium 1100–2100, thus gaining insights into drought hazards in historical and future time. Specifically, we detect the occurrence of exceptionally severe dry periods during MCA, Renaissance, and late LIA, which lasted for at least 40 years. These droughts seem to be more extreme than the dry periods that were observed during the instrumental time span (1807–2023). Notably, climate models consistently project a declining trend of mean river flow in the future, whose average value may turn out to be lower than the driest condition depicted by reconstruction and paleo-climate simulations. Moreover, annual and multidecadal drought conditions in the future will likely resemble, or even exceed, the worst event during MCA.

In addition, the compounding effects over the Po River basin of climate change and human activities—such as reduced water availability and rising water demand—are likely to further intensify future drought impacts (AghaKouchak et al., 2015, 2021). While our framework does not directly consider human impacts—which is less apparent compared to climatic drivers for the Po River flow at an annual time scale—it provides an essential first step toward better characterizing drought evolution within a millennium-long context, helping to advance our understanding of droughts in a warmer climate. Future studies could benefit from incorporating water-human system dynamic modeling (Davies & Simonovic, 2011) that accounts for both natural and human-driven processes, offering a more comprehensive understanding of interactions between the hydrological cycle and society (Van Loon, Stahl, et al., 2016; Quesada-Montano et al., 2018; AghaKouchak et al., 2021).

The satisfactory ability of climate models to reproduce past droughts does not of course imply that future projections will become true. However, the consistent indications provided by reconstruction and climate models in the simulation of past drought events and the occurrence of several important droughts in the Po River basin in the past 20 years (Montanari et al., 2023) indicate that the projections presented here of future drought hazard should be duly considered. Given that the continuously increasing temperature will likely amplify the impact of drought events, adaptation strategies are urgently needed to cope with future drought risk in the Po River basin and Alpine regions in general. There are, in particular, two socio-economic sectors that largely depend on the Po River and that should implement adaptation measures in response to the evolving drought hazard that our study exposes. First, both hydropower and thermopower sectors are particularly vulnerable to prolonged droughts; a vulnerability that warrants interventions aimed to increase power supply and reduce the financial exposure of power producers during dry spells (Chowdhury et al., 2023). Examples include the deployment of renewables that are less influenced by water availability (e.g., wind, solar), the construction of power transmission corridors, or the re-design of power market mechanisms. A second sector that has been, and will be, profoundly affected by evolving drought hazard is the agricultural one (Straffelini & Tarolli, 2023; Monteleone et al., 2023). In this case, adaptation measures are already in place, although one may wonder whether such measures are adequate given the magnitude and duration of the events that are likely to hit the Po Valley. There are also several environmental aspects that should also be taken into account: saline intrusion in the river delta causes major impacts on the river ecosystem (Tarolli et al., 2023), in turn requiring a discussion on Minimum Environmental Flow regulations.

The Po River is a favorable case for the availability of an extremely long time series of river flow observations and several historical reconstructions of flood rich and drought rich periods. This information allows to perform a suite of cross-validation tests offering solid support to the reliability of future drought hazard assessment. On the other hand, the tree-ring-based drought atlas, PMIP4, and CMIP6 simulations are available at the global level and therefore the framework herein proposed is potentially applicable to other catchments. Where there is a drought atlas, i.e., Asia (E. R. Cook, Anchukaitis, et al., 2010), Europe (E. R. Cook et al., 2015, 2020), eastern Australia and New Zealand (Palmer et al., 2015), North America (E. R. Cook, Seager, et al., 2010), and southern South America (Morales et al., 2020), there is potential to conveniently reconstruct river flows and integrate reconstructions with GCM outputs by reapplying our framework. A possible challenge would be the lack of long-term river flow observation data (40 years or more, depending on the statistical behaviors of the time series) for calibrating the reconstruction model. If river flow observations and other information that have been used for the case of the Po River are not available, it is still possible to cross-validate reconstructions with GCM simulations and other case-specific information that may be available (e.g., reanalysis or satellite dataset).

Note that the reliability of GCMs to simulate river flow has been tested here with respect to a large catchment (70,000 km^2) at the annual time scale, for which the results are encouraging. Note, also, that the annual temporal resolution of the drought atlas does not allow us to apply our framework to intrannual time scales, such as monthly or seasonal. Given that the GCMs are interpolated over a 0.25-degree grid, the framework is potentially applicable to smaller basins. However, we emphasize that cross-validation based on local data and information becomes more and more essential with decreasing spatial scales.

Overall, our approach shows that by combining instrumental records with paleohydrological reconstructions and climate projections, we can better characterize the evolution of droughts, ultimately providing the knowledge base necessary to inform future adaptation measures.

Conflict of Interest

The authors declare no competing interests.

Data availability

All data needed to evaluate the conclusions in the paper are publicly available. Specifically, the monthly time series of the Po River flows from January of 1807 to August of 2022 (Zanchetin, 2022) is available in Zenodo at https://doi.org/10.5281/zenodo.7225698. Additionally, for the period spanning September 2022 to December 2023, the online daily streamflow record for the Po River at Pontelagoscuro can be downloaded from https://simc.arpae.it/dext3r/. Old World Drought Altas (Cook, 2015) is available from https://www.ncei.noaa.gov/access/paleo-search/study/19419. PMIP4 data are publicly available from https://esgf-node.llnl.gov/search/cmip6/. CMIP6 data are derived from https://cds.climate.copernicus.eu/datasets/projections-cmip6?tab=download.

Acknowledgments

RG was supported by the China Scholarship Council (CSC) Scholarship (NO.202106060061) and Ministero degli Affari Esteri e della Cooperazione Internazionale (MAECI). HN is supported by the US National Science Foundation grant AGS-2302668. This study was carried out within the RETURN Extended Partnership and received funding from the European Union Next-GenerationEU (National Recovery and Resilience Plan – NRRP, Mission 4, Component 2, Investment 1.3 – D.D. 1243 2/8/2022, PE0000005).

References

AghaKouchak, A., Feldman, D., Hoerling, M., Huxman, T., & Lund, J. (2015). Water and climate: Recognize anthropogenic drought. *Nature*, *524*(7566), 409–411. doi: 10.1038/524409a

AghaKouchak, A., Mirchi, A., Madani, K., Di Baldassarre, G., Nazemi, A., Alborzi, A., … Wanders, N. (2021). Anthropogenic Drought: Definition, Challenges, and Opportunities. *Reviews of Geophysics*, *59*(2), e2019RG000683. doi: 10.1029/2019RG000683

Ault, T. R. (2020). On the essentials of drought in a changing climate. *Science*, *368*(6488), 256–260.

Ault, T. R., Cole, J. E., Overpeck, J. T., Pederson, G. T., George, S. S., Otto-Bliesner, B., … Deser, C. (2013). The continuum of hydroclimate variability in western North America during the last millennium. *Journal of Climate*, *26*(16), 5863–5878.

Ault, T. R., Cole, J. E., Overpeck, J. T., Pederson, G. T., & Meko, D. M. (2014). Assessing the risk of persistent drought using climate model simulations and paleoclimate data. *Journal of Climate*, *27*(20), 7529–7549.

Autorità di Bacino del Fiume Po. (2006). Caratteristiche del bacino del fiume Po e primo esame dell'impatto ambientale delle attività umane sulle risorse idriche. *Parma: Autoritá di bacino del fiume Po*.

Avanzi, F., Munerol, F., Milelli, M., Gabellani, S., Massari, C., Girotto, M., … others (2024). Winter snow deficit was a harbinger of summer 2022 socio-hydrologic drought in the Po Basin, Italy. *Communications Earth & Environment*, *5*(1), 64.

Blöschl, G., Kiss, A., Viglione, A., Barriendos, M., Böhm, O., Brázdil, R., … others (2020). Current European flood-rich period exceptional compared with past 500 years. *Nature*, *583*(7817), 560–566.

Büntgen, U., Tegel, W., Nicolussi, K., McCormick, M., Frank, D., Trouet, V., … others (2011). 2500 years of European climate variability and human susceptibility. *science*, *331*(6017), 578–582.

Büntgen, U., Urban, O., Krusic, P. J., Rybníček, M., Kolář, T., Kyncl, T., … others (2021). Recent European drought extremes beyond Common Era background variability. *Nature Geoscience*, *14*(4), 190–196.

Cannon, A. J., Sobie, S. R., & Murdock, T. Q. (2015). Bias correction of GCM precipitation by quantile mapping: How well do methods preserve changes in quantiles and extremes? *Journal of Climate*, *28*(17), 6938–6959.

Chen, F., Man, W., Wang, S., Esper, J., Meko, D., Büntgen, U., ... others (2023). Southeast Asian ecological dependency on Tibetan Plateau streamflow over the last millennium. *Nature Geoscience*, 1–8.

Chowdhury, A. K., Wild, T., Deshmukh, R., Iyer, G., & Galelli, S. (2023). Geophysical constraints on decarbonized systems—building spatio-temporal uncertainties into future electricity grid planning. *Current Sustainable/Renewable Energy Reports*, *10*(4), 218–233.

Cook, B. I., Ault, T. R., & Smerdon, J. E. (2015). Unprecedented 21st century drought risk in the american southwest and central plains. *Science Advances*, *1*(1), e1400082.

Cook, B. I., Cook, E. R., Smerdon, J. E., Seager, R., Williams, A. P., Coats, S., ... Díaz, J. V. (2016). North american megadroughts in the common era: Reconstructions and simulations. *Wiley Interdisciplinary Reviews: Climate Change*, *7*(3), 411–432.

Cook, B. I., Smerdon, J. E., Cook, E. R., Williams, A. P., Anchukaitis, K. J., Mankin, J. S., ... others (2022). Megadroughts in the common era and the anthropocene. *Nature Reviews Earth & Environment*, *3*(11), 741–757.

Cook, E. R., Anchukaitis, K. J., Buckley, B. M., D'Arrigo, R. D., Jacoby, G. C., & Wright, W. E. (2010). Asian monsoon failure and megadrought during the last millennium. *Science*, *328*(5977), 486–489.

Cook, E. R., & Kairiukstis, L. A. (2013). *Methods of dendrochronology: Applications in the environmental sciences.* Springer Science & Business Media.

Cook, E. R., Seager, R., Heim Jr, R. R., Vose, R. S., Herweijer, C., & Woodhouse, C. (2010). Megadroughts in North America: Placing IPCC projections of hydroclimatic change in a long-term palaeoclimate context. *Journal of Quaternary Science*, *25*(1), 48–61.

Cook, E. R., Seager, R., Kushnir, Y., Briffa, K. R., Büntgen, U., Frank, D., ... others (2015). Old world megadroughts and pluvials during the common era. *Science advances*, *1*(10), e1500561.

Cook, E. R., Solomina, O., Matskovsky, V., Cook, B. I., Agafonov, L., Berdnikova, A., ... Yermokhin, M. (2020). The European Russia Drought Atlas (1400–2016 CE). *Climate Dynamics*, *54*(3), 2317–2335. doi: 10.1007/s00382-019-05115-2

Coulthard, B., Smith, D. J., & Meko, D. M. (2016). Is worst-case scenario streamflow drought underestimated in British Columbia? A multi-century perspective for the south coast, derived from tree-rings. *Journal of Hydrology*, *534*, 205–218. doi: 10.1016/j.jhydrol.2015.12.030

Davies, E. G. R., & Simonovic, S. P. (2011). Global water resources modeling with an integrated model of the social–economic–environmental system. *Advances in Water Resources*, *34*(6), 684–700. doi: 10.1016/j.advwatres.2011.02.010

Di Baldassarre, G., Wanders, N., AghaKouchak, A., Kuil, L., Rangecroft, S., Veldkamp, T. I. E., ... Van Loon, A. F. (2018). Water shortages worsened by reservoir effects. *Nature Sustainability*, *1*(11), 617–622. doi: 10.1038/s41893-018-0159-0

Essa, Y. H., Hirschi, M., Thiery, W., El-Kenawy, A. M., & Yang, C. (2023). Drought characteristics in Mediterranean under future climate change. *npj Climate and Atmospheric Science*, *6*(1), 133.

Galelli, S., Nguyen, H. T. T., Turner, S. W. D., & Buckley, B. M. (2021). Time to Use Dendrohydrological Data in Water Resources Management? *Journal of Water Resources Planning and Management*, *147*(8), 01821001. doi: 10.1061/(ASCE)WR.1943-5452.0001422

Genuer, R., Poggi, J.-M., & Tuleau-Malot, C. (2010). Variable selection using random forests. *Pattern recognition letters*, *31*(14), 2225–2236.

Giovannelli, E., & Allodi, G. (1960). Il Po a Pontelagoscuro—Scale delle portate e valori giornalieri e mensili pel venticinquennio 1917–1941. *Internal Report of the National Hydrographic Service of Italy*.

Guo, R., & Montanari, A. (2023). Historical rainfall data in northern Italy predict larger meteorological drought hazard than climate projections. *Hydrology and Earth System Sciences*, *27*(15), 2847–2863.

Gupta, H. V., Kling, H., Yilmaz, K. K., & Martinez, G. F. (2009). Decomposition of the mean squared error and NSE performance criteria: Implications for improving hydrological modelling. *Journal of hydrology*, *377*(1-2), 80–91.

Helama, S., Meriläinen, J., & Tuomenvirta, H. (2009). Multicentennial megadrought in northern europe coincided with a global el niño–southern oscillation drought pattern during the medieval climate anomaly. *Geology*, *37*(2), 175–178.

Hessl, A. E., Anchukaitis, K. J., Jelsema, C., Cook, B., Byambasuren, O., Leland, C., … Hayles, L. A. (2018). Past and future drought in Mongolia. *Science advances*, *4*(3), e1701832.

Hidalgo, H. G., Piechota, T. C., & Dracup, J. A. (2000). Alternative principal components regression procedures for dendrohydrologic reconstructions. *Water Resources Research*, *36*(11), 3241–3249.

Ho, M., Lall, U., & Cook, E. R. (2016). Can a paleodrought record be used to reconstruct streamflow?: A case study for the Missouri River Basin. *Water Resources Research*, *52*(7), 5195–5212.

Ho, M., Lall, U., Sun, X., & Cook, E. R. (2017). Multiscale temporal variability and regional patterns in 555 years of conterminous US streamflow. *Water Resources Research*, *53*(4), 3047–3066.

Ionita, M., Dima, M., Nagavciuc, V., Scholz, P., & Lohmann, G. (2021). Past megadroughts in central Europe were longer, more severe and less warm than modern droughts. *Communications Earth & Environment*, *2*(1), 61.

IPCC. (2021). Summary for Policymakers. In V. Masson-Delmotte et al. (Eds.), *Climate Change 2021: The Physical Science Basis. Contribution of Working Group I to the Sixth Assessment Report of the Intergovernmental Panel on Climate Change* (pp. 3–32). Cambridge, United Kingdom and New York, NY, USA: Cambridge University Press. doi: 10.1017/9781009157896.001

Jungclaus, J. H., Bard, E., Baroni, M., Braconnot, P., Cao, J., Chini, L. P., … others (2017). The PMIP4 contribution to CMIP6–Part 3: The last millennium, scientific objective, and experimental design for the PMIP4 past1000 simulations. *Geoscientific Model Development*, *10*(11), 4005–4033.

Kageyama, M., Braconnot, P., Harrison, S. P., Haywood, A. M., Jungclaus, J. H., Otto-Bliesner, B. L., … others (2018). The PMIP4 contribution to CMIP6–Part 1: Overview and over-arching analysis plan. *Geoscientific Model Development*, *11*(3), 1033–1057.

Khan, N., Nguyen, H. T., Galelli, S., & Cherubini, P. (2022). Increasing drought risks over the past four centuries amidst projected flood intensification in the kabul river basin (afghanistan and pakistan)—evidence from tree rings. *Geophysical Research Letters*, *49*(24), e2022GL100703.

Knoben, W. J., Woods, R. A., & Freer, J. E. (2018). A quantitative hydrological climate classification evaluated with independent streamflow data. *Water Resources Research*, *54*(7), 5088–5109.

Koutsoyiannis, D., & Montanari, A. (2022). Bluecat: A local uncertainty estimator for deterministic simulations and predictions. *Water Resources Research*, *58*(1), e2021WR031215.

Li, X., Long, D., Scanlon, B. R., Mann, M. E., Li, X., Tian, F., … Wang, G. (2022). Climate change threatens terrestrial water storage over the Tibetan Plateau. *Nature Climate Change*, *12*(9), 801–807.

Lund, J., Medellin-Azuara, J., Durand, J., & Stone, K. (2018). Lessons from california's 2012–2016 drought. *Journal of Water Resources Planning and Manage-*

ment, *144*(10), 04018067.

Marani, M., & Zanetti, S. (2015). Long-term oscillations in rainfall extremes in a 268 year daily time series. *Water Resources Research*, *51*(1), 639–647.

Massey Jr, F. J. (1951). The Kolmogorov-Smirnov test for goodness of fit. *Journal of the American statistical Association*, *46*(253), 68–78.

Montanari, A. (2012). Hydrology of the Po River: Looking for changing patterns in river discharge. *Hydrology and Earth System Sciences*, *16*(10), 3739–3747.

Montanari, A., Nguyen, H., Rubinetti, S., Ceola, S., Galelli, S., Rubino, A., & Zanchettin, D. (2023). Why the 2022 Po River drought is the worst in the past two centuries. *Science Advances*, *9*(32), eadg8304.

Monteleone, B., Borzí, I., Arosio, M., Cesarini, L., Bonaccorso, B., & Martina, M. (2023). Modelling the response of wheat yield to stage-specific water stress in the Po Plain. *Agricultural Water Management*, *287*, 108444.

Morales, M. S., Cook, E. R., Barichivich, J., Christie, D. A., Villalba, R., LeQuesne, C., … Boninsegna, J. A. (2020). Six hundred years of South American tree rings reveal an increase in severe hydroclimatic events since mid-20th century. *Proceedings of the National Academy of Sciences*, *117*(29), 16816–16823. doi: 10.1073/pnas.2002411117

Nash, J. E., & Sutcliffe, J. V. (1970). River flow forecasting through conceptual models part I—A discussion of principles. *Journal of hydrology*, *10*(3), 282–290.

Nguyen, H. T., & Galelli, S. (2018). A linear dynamical systems approach to streamflow reconstruction reveals history of regime shifts in northern Thailand. *Water Resources Research*, *54*(3), 2057–2077.

Nguyen, H. T., Turner, S. W., Buckley, B. M., & Galelli, S. (2020). Coherent streamflow variability in monsoon Asia over the past eight centuries—Links to oceanic drivers. *Water Resources Research*, *56*(12), e2020WR027883.

O'Neill, B. C., Tebaldi, C., van Vuuren, D. P., Eyring, V., Friedlingstein, P., Hurtt, G., … Sanderson, B. M. (2016). The Scenario Model Intercomparison Project (ScenarioMIP) for CMIP6. *Geoscientific Model Development*, *9*(9), 3461–3482. doi: 10.5194/gmd-9-3461-2016

PAGES Hydro2k Consortium. (2017). Comparing proxy and model estimates of hydroclimate variability and change over the Common Era. *Climate of the Past*, *13*(12), 1851–1900.

Palmer, J. G., Cook, E. R., Turney, C. S. M., Allen, K., Fenwick, P., Cook, B. I., … Baker, P. (2015). Drought variability in the eastern Australia and New Zealand summer drought atlas (ANZDA, CE 1500–2012) modulated by the Interdecadal Pacific Oscillation. *Environmental Research Letters*, *10*(12), 124002. doi: 10.1088/1748-9326/10/12/124002

Potter, E. R., Fyffe, C. L., Orr, A., Quincey, D. J., Ross, A. N., Rangecroft, S., … others (2023). A future of extreme precipitation and droughts in the Peruvian Andes. *npj Climate and Atmospheric Science*, *6*(1), 96.

Quesada-Montano, B., Di Baldassarre, G., Rangecroft, S., & Van Loon, A. F. (2018). Hydrological change: Towards a consistent approach to assess changes on both floods and droughts. *Advances in Water Resources*, *111*, 31–35. doi: 10.1016/j.advwatres.2017.10.038

Rao, M. P., Cook, E. R., Cook, B. I., D'Arrigo, R. D., Palmer, J. G., Lall, U., … others (2020). Seven centuries of reconstructed Brahmaputra River discharge demonstrate underestimated high discharge and flood hazard frequency. *Nature communications*, *11*(1), 6017.

Rubinetti, S., Taricco, C., Alessio, S., Rubino, A., Bizzarri, I., & Zanchettin, D. (2020). Robust decadal hydroclimate predictions for northern italy based on a twofold statistical approach. *Atmosphere*, *11*(6), 671.

Sousa, P. M., Blamey, R. C., Reason, C. J., Ramos, A. M., & Trigo, R. M. (2018). The 'Day Zero'Cape Town drought and the poleward migration of moisture corridors. *Environmental Research Letters*, *13*(12), 124025.

Stahl, K., Kohn, I., Blauhut, V., Urquijo, J., De Stefano, L., Acácio, V., ... others (2016). Impacts of European drought events: Insights from an international database of text-based reports. *Natural Hazards and Earth System Sciences*, *16*(3), 801–819.

Straffelini, E., & Tarolli, P. (2023). Climate change-induced aridity is affecting agriculture in Northeast Italy. *Agricultural Systems*, *208*, 103647.

Taricco, C., Alessio, S., Rubinetti, S., Zanchettin, D., Cosoli, S., Gačić, M., ... Rubino, A. (2015). Marine sediments remotely unveil long-term climatic variability over Northern Italy. *Scientific reports*, *5*(1), 12111.

Tarolli, P., Luo, J., Straffelini, E., Liou, Y.-A., Nguyen, K.-A., Laurenti, R., ... D'Agostino, V. (2023). Saltwater intrusion and climate change impact on coastal agriculture. *Plos Water*, *2*(4), e0000121.

Terrell, G. R., & Scott, D. W. (1992). Variable kernel density estimation. *The Annals of Statistics*, 1236–1265.

Ukkola, A. M., De Kauwe, M. G., Roderick, M. L., Abramowitz, G., & Pitman, A. J. (2020). Robust future changes in meteorological drought in CMIP6 projections despite uncertainty in precipitation. *Geophysical Research Letters*, *47*(11), e2020GL087820.

Van Dijk, A. I., Beck, H. E., Crosbie, R. S., De Jeu, R. A., Liu, Y. Y., Podger, G. M., ... Viney, N. R. (2013). The Millennium Drought in southeast Australia (2001–2009): Natural and human causes and implications for water resources, ecosystems, economy, and society. *Water Resources Research*, *49*(2), 1040–1057.

Van Loon, A. F., Gleeson, T., Clark, J., Van Dijk, A. I. J. M., Stahl, K., Hannaford, J., ... Van Lanen, H. A. J. (2016). Drought in the Anthropocene. *Nature Geoscience*, *9*(2), 89–91. doi: 10.1038/ngeo2646

Van Loon, A. F., & Laaha, G. (2015). Hydrological drought severity explained by climate and catchment characteristics. *Journal of hydrology*, *526*, 3–14.

Van Loon, A. F., Stahl, K., Di Baldassarre, G., Clark, J., Rangecroft, S., Wanders, N., ... Van Lanen, H. A. J. (2016). Drought in a human-modified world: Reframing drought definitions, understanding, and analysis approaches. *Hydrology and Earth System Sciences*, *20*(9), 3631–3650. doi: 10.5194/hess-20-3631-2016

Wells, N., Goddard, S., & Hayes, M. J. (2004). A self-calibrating Palmer drought severity index. *Journal of climate*, *17*(12), 2335–2351.

Wu, Y., Long, D., Lall, U., Scanlon, B. R., Tian, F., Fu, X., ... Hu, C. (2022). Reconstructed eight-century streamflow in the Tibetan Plateau reveals contrasting regional variability and strong nonstationarity. *Nature Communications*, *13*(1), 6416.

Yevjevich, V. (1967). *An objective approach to definitions and investigations of continental hydrologic droughts* (Unpublished doctoral dissertation). Hydrology Paper23, Colorado State University, Fort Collins.

Zanchettin, D., Rubino, A., Traverso, P., & Tomasino, M. (2008). Impact of variations in solar activity on hydrological decadal patterns in northern Italy. *Journal of Geophysical Research: Atmospheres*, *113*(D12).

Zanchettin, D., Traverso, P., & Tomasino, M. (2008). Po River discharges: A preliminary analysis of a 200-year time series. *Climatic Change*, *89*(3-4), 411–433.

Cook, E. R. (2015). *Paleoclimatology - Old World Drought Atlas [Dataset].* NOAA National Centers for Environmental Information. Retrieved from `https://doi.org/10.25921/rjm6-mq74`

Zanchetin, D. (2022). *Monthly Discharge of Po River at Pontelagoscuro [Dataset].* Zenodo. Retrieved from `https://doi.org/10.5281/zenodo.7225699`

References from the Supporting Materials

Bentsen, M., Oliviè, D. J. L., Seland, y., Toniazzo, T., Gjermundsen, A., Graff, L. S., … Schulz, M. (2019a). *NCC NorESM2-MM model output prepared for CMIP6 CMIP historical.* Earth System Grid Federation. Retrieved from https://doi.org/10.22033/ESGF/CMIP6.8040 doi: 10.22033/ESGF/CMIP6.8040

Bentsen, M., Oliviè, D. J. L., Seland, y., Toniazzo, T., Gjermundsen, A., Graff, L. S., … Schulz, M. (2019b). *NCC NorESM2-MM model output prepared for CMIP6 ScenarioMIP ssp126.* Earth System Grid Federation. Retrieved from https://doi.org/10.22033/ESGF/CMIP6.8250 doi: 10.22033/ESGF/CMIP6.8250

Bentsen, M., Oliviè, D. J. L., Seland, y., Toniazzo, T., Gjermundsen, A., Graff, L. S., … Schulz, M. (2019c). *NCC NorESM2-MM model output prepared for CMIP6 ScenarioMIP ssp585.* Earth System Grid Federation. Retrieved from https://doi.org/10.22033/ESGF/CMIP6.8321 doi: 10.22033/ESGF/CMIP6.8321

Boucher, O., Denvil, S., Levavasseur, G., Cozic, A., Caubel, A., Foujols, M.-A., … Cheruy, F. (2018). *IPSL IPSL-CM6A-LR model output prepared for CMIP6 CMIP historical.* Earth System Grid Federation. Retrieved from https://doi.org/10.22033/ESGF/CMIP6.5195 doi: 10.22033/ESGF/CMIP6.5195

Boucher, O., Denvil, S., Levavasseur, G., Cozic, A., Caubel, A., Foujols, M.-A., … Lurton, T. (2019a). *IPSL IPSL-CM6A-LR model output prepared for CMIP6 ScenarioMIP ssp126.* Earth System Grid Federation. Retrieved from https://doi.org/10.22033/ESGF/CMIP6.5262 doi: 10.22033/ESGF/CMIP6.5262

Boucher, O., Denvil, S., Levavasseur, G., Cozic, A., Caubel, A., Foujols, M.-A., … Lurton, T. (2019b). *IPSL IPSL-CM6A-LR model output prepared for CMIP6 ScenarioMIP ssp585.* Earth System Grid Federation. Retrieved from https://doi.org/10.22033/ESGF/CMIP6.5271 doi: 10.22033/ESGF/CMIP6.5271

Danabasoglu, G. (2019a). *NCAR CESM2 model output prepared for CMIP6 CMIP historical.* Earth System Grid Federation. Retrieved from https://doi.org/10.22033/ESGF/CMIP6.7627 doi: 10.22033/ESGF/CMIP6.7627

Danabasoglu, G. (2019b). *NCAR CESM2 model output prepared for CMIP6 ScenarioMIP ssp126.* Earth System Grid Federation. Retrieved from https://doi.org/10.22033/ESGF/CMIP6.7746 doi: 10.22033/ESGF/CMIP6.7746

Danabasoglu, G. (2019c). *NCAR CESM2 model output prepared for CMIP6 ScenarioMIP ssp585.* Earth System Grid Federation. Retrieved from https://doi.org/10.22033/ESGF/CMIP6.7768 doi: 10.22033/ESGF/CMIP6.7768

Dix, M., Bi, D., Dobrohotoff, P., Fiedler, R., Harman, I., Law, R., … Yang, R. (2019a). *CSIRO-ARCCSS ACCESS-CM2 model output prepared for CMIP6 CMIP historical.* Earth System Grid Federation. Retrieved from https://doi.org/10.22033/ESGF/CMIP6.4271 doi: 10.22033/ESGF/CMIP6.4271

Dix, M., Bi, D., Dobrohotoff, P., Fiedler, R., Harman, I., Law, R., … Yang, R. (2019b). *CSIRO-ARCCSS ACCESS-CM2 model output prepared for CMIP6 ScenarioMIP ssp126.* Earth System Grid Federation. Retrieved from https://doi.org/10.22033/ESGF/CMIP6.4319 doi: 10.22033/ESGF/CMIP6.4319

Dix, M., Bi, D., Dobrohotoff, P., Fiedler, R., Harman, I., Law, R., … Yang, R. (2019c). *CSIRO-ARCCSS ACCESS-CM2 model output prepared for CMIP6 ScenarioMIP ssp585.* Earth System Grid Federation. Retrieved from https://doi.org/10.22033/ESGF/CMIP6.4332 doi: 10.22033/ESGF/CMIP6.4332

EC-Earth, E.-E. C. (2020a). *EC-Earth-Consortium EC-Earth3-Veg-LR model output prepared for CMIP6 CMIP historical.* Earth System Grid Federation. Retrieved from https://doi.org/10.22033/ESGF/CMIP6.4707 doi: 10.22033/ESGF/CMIP6.4707

EC-Earth, E.-E. C. (2020b). *EC-Earth-Consortium EC-Earth3-Veg-LR model output* *prepared for CMIP6 ScenarioMIP ssp126.* Earth System Grid Federation. Retrieved from https://doi.org/10.22033/ESGF/CMIP6.4877 doi: 10.22033/ESGF/CMIP6.4877

EC-Earth, E.-E. C. (2020c). *EC-Earth-Consortium EC-Earth3-Veg-LR model output prepared for CMIP6 ScenarioMIP ssp585.* Earth System Grid Federation. Retrieved from https://doi.org/10.22033/ESGF/CMIP6.4915 doi: 10.22033/ESGF/CMIP6.4915

Good, P. (2020a). *MOHC HadGEM3-GC31-LL model output prepared for CMIP6 ScenarioMIP ssp126.* Earth System Grid Federation. Retrieved from https://doi.org/10.22033/ESGF/CMIP6.10849 doi: 10.22033/ESGF/CMIP6.10849

Good, P. (2020b). *MOHC HadGEM3-GC31-LL model output prepared for CMIP6 ScenarioMIP ssp585.* Earth System Grid Federation. Retrieved from https://doi.org/10.22033/ESGF/CMIP6.10901 doi: 10.22033/ESGF/CMIP6.10901

Good, P., Sellar, A., Tang, Y., Rumbold, S., Ellis, R., Kelley, D., & Kuhlbrodt, T. (2019a). *MOHC UKESM1.0-LL model output prepared for CMIP6 ScenarioMIP ssp126.* Earth System Grid Federation. Retrieved from https://doi.org/10.22033/ESGF/CMIP6.6333 doi: 10.22033/ESGF/CMIP6.6333

Good, P., Sellar, A., Tang, Y., Rumbold, S., Ellis, R., Kelley, D., & Kuhlbrodt, T. (2019b). *MOHC UKESM1.0-LL model output prepared for CMIP6 ScenarioMIP ssp585.* Earth System Grid Federation. Retrieved from https://doi.org/10.22033/ESGF/CMIP6.6405 doi: 10.22033/ESGF/CMIP6.6405

Hajima, T., Abe, M., Arakawa, O., Suzuki, T., Komuro, Y., Ogura, T., … Tachiiri, K. (2019). *MIROC MIROC-ES2L model output prepared for CMIP6 CMIP historical.* Earth System Grid Federation. Retrieved from https://doi.org/10.22033/ESGF/CMIP6.5602 doi: 10.22033/ESGF/CMIP6.5602

Huang, W. (2019a). *THU CIESM model output prepared for CMIP6 CMIP historical.* Earth System Grid Federation. Retrieved from https://doi.org/10.22033/ESGF/CMIP6.8843 doi: 10.22033/ESGF/CMIP6.8843

Huang, W. (2019b). *THU CIESM model output prepared for CMIP6 ScenarioMIP ssp126.* Earth System Grid Federation. Retrieved from https://doi.org/10.22033/ESGF/CMIP6.8857 doi: 10.22033/ESGF/CMIP6.8857

Huang, W. (2020). *THU CIESM model output prepared for CMIP6 ScenarioMIP ssp585.* Earth System Grid Federation. Retrieved from https://doi.org/10.22033/ESGF/CMIP6.8863 doi: 10.22033/ESGF/CMIP6.8863

Kim, Y., Noh, Y., Kim, D., Lee, M.-I., Lee, H. J., Kim, S. Y., & Kim, D. (2019a). *KIOST KIOST-ESM model output prepared for CMIP6 CMIP historical.* Earth System Grid Federation. Retrieved from https://doi.org/10.22033/ESGF/CMIP6.5296 doi: 10.22033/ESGF/CMIP6.5296

Kim, Y., Noh, Y., Kim, D., Lee, M.-I., Lee, H. J., Kim, S. Y., & Kim, D. (2019b). *KIOST KIOST-ESM model output prepared for CMIP6 ScenarioMIP ssp126.* Earth System Grid Federation. Retrieved from https://doi.org/10.22033/ESGF/CMIP6.11243 doi: 10.22033/ESGF/CMIP6.11243

Kim, Y., Noh, Y., Kim, D., Lee, M.-I., Lee, H. J., Kim, S. Y., & Kim, D. (2019c). *KIOST KIOST-ESM model output prepared for CMIP6 ScenarioMIP ssp585.* Earth System Grid Federation. Retrieved from https://doi.org/10.22033/ESGF/CMIP6.11249 doi: 10.22033/ESGF/CMIP6.11249

Lee, W.-L., & Liang, H.-C. (2020a). *AS-RCEC TaiESM1.0 model output prepared for CMIP6 CMIP historical.* Earth System Grid Federation. Retrieved from https://doi.org/10.22033/ESGF/CMIP6.9755 doi: 10.22033/ESGF/CMIP6.9755

Lee, W.-L., & Liang, H.-C. (2020b). *AS-RCEC TaiESM1.0 model output prepared for CMIP6 ScenarioMIP ssp126.* Earth System Grid Federation. Retrieved from https://doi.org/10.22033/ESGF/CMIP6.9806 doi: 10.22033/ESGF/CMIP6.9806

Lee, W.-L., & Liang, H.-C. (2020c). *AS-RCEC TaiESM1.0 model output prepared* *for CMIP6 ScenarioMIP ssp585.* Earth System Grid Federation. Retrieved from `https://doi.org/10.22033/ESGF/CMIP6.9823` doi: 10.22033/ESGF/CMIP6.9823

Lovato, T., & Peano, D. (2020a). *CMCC CMCC-CM2-SR5 model output prepared for CMIP6 CMIP historical.* Earth System Grid Federation. Retrieved from `https://doi.org/10.22033/ESGF/CMIP6.3825` doi: 10.22033/ESGF/CMIP6.3825

Lovato, T., & Peano, D. (2020b). *CMCC CMCC-CM2-SR5 model output prepared for CMIP6 ScenarioMIP ssp126.* Earth System Grid Federation. Retrieved from `https://doi.org/10.22033/ESGF/CMIP6.3887` doi: 10.22033/ESGF/CMIP6.3887

Lovato, T., & Peano, D. (2020c). *CMCC CMCC-CM2-SR5 model output prepared for CMIP6 ScenarioMIP ssp585.* Earth System Grid Federation. Retrieved from `https://doi.org/10.22033/ESGF/CMIP6.3896` doi: 10.22033/ESGF/CMIP6.3896

Lovato, T., Peano, D., & Butenschön, M. (2021a). *CMCC CMCC-ESM2 model output prepared for CMIP6 CMIP historical.* Earth System Grid Federation. Retrieved from `https://doi.org/10.22033/ESGF/CMIP6.13195` doi: 10.22033/ESGF/CMIP6.13195

Lovato, T., Peano, D., & Butenschön, M. (2021b). *CMCC CMCC-ESM2 model output prepared for CMIP6 ScenarioMIP ssp126.* Earth System Grid Federation. Retrieved from `https://doi.org/10.22033/ESGF/CMIP6.13250` doi: 10.22033/ESGF/CMIP6.13250

Lovato, T., Peano, D., & Butenschön, M. (2021c). *CMCC CMCC-ESM2 model output prepared for CMIP6 ScenarioMIP ssp585.* Earth System Grid Federation. Retrieved from `https://doi.org/10.22033/ESGF/CMIP6.13259` doi: 10.22033/ESGF/CMIP6.13259

Ridley, J., Menary, M., Kuhlbrodt, T., Andrews, M., & Andrews, T. (2019). *MOHC HadGEM3-GC31-LL model output prepared for CMIP6 CMIP historical.* Earth System Grid Federation. Retrieved from `https://doi.org/10.22033/ESGF/CMIP6.6109` doi: 10.22033/ESGF/CMIP6.6109

Seferian, R. (2018). *CNRM-CERFACS CNRM-ESM2-1 model output prepared for CMIP6 CMIP historical.* Earth System Grid Federation. Retrieved from `https://doi.org/10.22033/ESGF/CMIP6.4068` doi: 10.22033/ESGF/CMIP6.4068

Seland, y., Bentsen, M., Oliviè, D. J. L., Toniazzo, T., Gjermundsen, A., Graff, L. S., … Schulz, M. (2019a). *NCC NorESM2-LM model output prepared for CMIP6 CMIP historical.* Earth System Grid Federation. Retrieved from `https://doi.org/10.22033/ESGF/CMIP6.8036` doi: 10.22033/ESGF/CMIP6.8036

Seland, y., Bentsen, M., Oliviè, D. J. L., Toniazzo, T., Gjermundsen, A., Graff, L. S., … Schulz, M. (2019b). *NCC NorESM2-LM model output prepared for CMIP6 ScenarioMIP ssp126.* Earth System Grid Federation. Retrieved from `https://doi.org/10.22033/ESGF/CMIP6.8248` doi: 10.22033/ESGF/CMIP6.8248

Seland, y., Bentsen, M., Oliviè, D. J. L., Toniazzo, T., Gjermundsen, A., Graff, L. S., … Schulz, M. (2019c). *NCC NorESM2-LM model output prepared for CMIP6 ScenarioMIP ssp585.* Earth System Grid Federation. Retrieved from `https://doi.org/10.22033/ESGF/CMIP6.8319` doi: 10.22033/ESGF/CMIP6.8319

Shiogama, H., Abe, M., & Tatebe, H. (2019a). *MIROC MIROC6 model output prepared for CMIP6 ScenarioMIP ssp126.* Earth System Grid Federation. Retrieved from `https://doi.org/10.22033/ESGF/CMIP6.5743` doi: 10.22033/ESGF/CMIP6.5743

Shiogama, H., Abe, M., & Tatebe, H. (2019b). *MIROC MIROC6 model output prepared for CMIP6 ScenarioMIP ssp585.* Earth System Grid Federation. Retrieved from https://doi.org/10.22033/ESGF/CMIP6.5771 doi: 10.22033/ESGF/CMIP6.5771

Stouffer, R. (2019a). *UA MCM-UA-1-0 model output prepared for CMIP6 CMIP historical.* Earth System Grid Federation. Retrieved from https://doi.org/10.22033/ESGF/CMIP6.8888 doi: 10.22033/ESGF/CMIP6.8888

Stouffer, R. (2019b). *UA MCM-UA-1-0 model output prepared for CMIP6 ScenarioMIP ssp126.* Earth System Grid Federation. Retrieved from https://doi.org/10.22033/ESGF/CMIP6.13895 doi: 10.22033/ESGF/CMIP6.13895

Stouffer, R. (2019c). *UA MCM-UA-1-0 model output prepared for CMIP6 ScenarioMIP ssp585.* Earth System Grid Federation. Retrieved from https://doi.org/10.22033/ESGF/CMIP6.13901 doi: 10.22033/ESGF/CMIP6.13901

Swart, N. C., Cole, J. N., Kharin, V. V., Lazare, M., Scinocca, J. F., Gillett, N. P., … Sigmond, M. (2019a). *CCCma CanESM5-CanOE model output prepared for CMIP6 CMIP historical.* Earth System Grid Federation. Retrieved from https://doi.org/10.22033/ESGF/CMIP6.10260 doi: 10.22033/ESGF/CMIP6.10260

Swart, N. C., Cole, J. N., Kharin, V. V., Lazare, M., Scinocca, J. F., Gillett, N. P., … Sigmond, M. (2019b). *CCCma CanESM5-CanOE model output prepared for CMIP6 ScenarioMIP ssp126.* Earth System Grid Federation. Retrieved from https://doi.org/10.22033/ESGF/CMIP6.10269 doi: 10.22033/ESGF/CMIP6.10269

Swart, N. C., Cole, J. N., Kharin, V. V., Lazare, M., Scinocca, J. F., Gillett, N. P., … Sigmond, M. (2019c). *CCCma CanESM5-CanOE model output prepared for CMIP6 ScenarioMIP ssp585.* Earth System Grid Federation. Retrieved from https://doi.org/10.22033/ESGF/CMIP6.10276 doi: 10.22033/ESGF/CMIP6.10276

Tachiiri, K., Abe, M., Hajima, T., Arakawa, O., Suzuki, T., Komuro, Y., … Kawamiya, M. (2019a). *MIROC MIROC-ES2L model output prepared for CMIP6 ScenarioMIP ssp126.* Earth System Grid Federation. Retrieved from https://doi.org/10.22033/ESGF/CMIP6.5742 doi: 10.22033/ESGF/CMIP6.5742

Tachiiri, K., Abe, M., Hajima, T., Arakawa, O., Suzuki, T., Komuro, Y., … Kawamiya, M. (2019b). *MIROC MIROC-ES2L model output prepared for CMIP6 ScenarioMIP ssp585.* Earth System Grid Federation. Retrieved from https://doi.org/10.22033/ESGF/CMIP6.5770 doi: 10.22033/ESGF/CMIP6.5770

Tang, Y., Rumbold, S., Ellis, R., Kelley, D., Mulcahy, J., Sellar, A., … Jones, C. (2019). *MOHC UKESM1.0-LL model output prepared for CMIP6 CMIP historical.* Earth System Grid Federation. Retrieved from https://doi.org/10.22033/ESGF/CMIP6.6113 doi: 10.22033/ESGF/CMIP6.6113

Tatebe, H., & Watanabe, M. (2018). *MIROC MIROC6 model output prepared for CMIP6 CMIP historical.* Earth System Grid Federation. Retrieved from https://doi.org/10.22033/ESGF/CMIP6.5603 doi: 10.22033/ESGF/CMIP6.5603

Voldoire, A. (2018). *CMIP6 simulations of the CNRM-CERFACS based on CNRM-CM6-1 model for CMIP experiment historical.* Earth System Grid Federation. Retrieved from https://doi.org/10.22033/ESGF/CMIP6.4066 doi: 10.22033/ESGF/CMIP6.4066

Voldoire, A. (2019a). *CNRM-CERFACS CNRM-CM6-1-HR model output prepared for CMIP6 CMIP historical.* Earth System Grid Federation. Retrieved from https://doi.org/10.22033/ESGF/CMIP6.4067 doi: 10.22033/ESGF/CMIP6.4067

Voldoire, A. (2019b). *CNRM-CERFACS CNRM-CM6-1-HR model output prepared for CMIP6 ScenarioMIP ssp585.* Earth System Grid Federation. Retrieved from https://doi.org/10.22033/ESGF/CMIP6.4225 doi: 10.22033/ESGF/

CMIP6.4225

Voldoire, A. (2019c). *CNRM-CERFACS CNRM-CM6-1 model output prepared for CMIP6 ScenarioMIP ssp126.* Earth System Grid Federation. Retrieved from https://doi.org/10.22033/ESGF/CMIP6.4184 doi: 10.22033/ESGF/CMIP6.4184

Voldoire, A. (2019d). *CNRM-CERFACS CNRM-CM6-1 model output prepared for CMIP6 ScenarioMIP ssp585.* Earth System Grid Federation. Retrieved from https://doi.org/10.22033/ESGF/CMIP6.4224 doi: 10.22033/ESGF/CMIP6.4224

Voldoire, A. (2019e). *CNRM-CERFACS CNRM-ESM2-1 model output prepared for CMIP6 ScenarioMIP ssp126.* Earth System Grid Federation. Retrieved from https://doi.org/10.22033/ESGF/CMIP6.4186 doi: 10.22033/ESGF/CMIP6.4186

Voldoire, A. (2019f). *CNRM-CERFACS CNRM-ESM2-1 model output prepared for CMIP6 ScenarioMIP ssp585.* Earth System Grid Federation. Retrieved from https://doi.org/10.22033/ESGF/CMIP6.4226 doi: 10.22033/ESGF/CMIP6.4226

Voldoire, A. (2020). *CNRM-CERFACS CNRM-CM6-1-HR model output prepared for CMIP6 ScenarioMIP ssp126.* Earth System Grid Federation. Retrieved from https://doi.org/10.22033/ESGF/CMIP6.4185 doi: 10.22033/ESGF/CMIP6.4185

Volodin, E., Mortikov, E., Gritsun, A., Lykossov, V., Galin, V., Diansky, N., … Emelina, S. (2019a). *INM INM-CM4-8 model output prepared for CMIP6 CMIP historical.* Earth System Grid Federation. Retrieved from https://doi.org/10.22033/ESGF/CMIP6.5069 doi: 10.22033/ESGF/CMIP6.5069

Volodin, E., Mortikov, E., Gritsun, A., Lykossov, V., Galin, V., Diansky, N., … Emelina, S. (2019b). *INM INM-CM4-8 model output prepared for CMIP6 ScenarioMIP ssp126.* Earth System Grid Federation. Retrieved from https://doi.org/10.22033/ESGF/CMIP6.12325 doi: 10.22033/ESGF/CMIP6.12325

Volodin, E., Mortikov, E., Gritsun, A., Lykossov, V., Galin, V., Diansky, N., … Emelina, S. (2019c). *INM INM-CM4-8 model output prepared for CMIP6 ScenarioMIP ssp585.* Earth System Grid Federation. Retrieved from https://doi.org/10.22033/ESGF/CMIP6.12337 doi: 10.22033/ESGF/CMIP6.12337

Volodin, E., Mortikov, E., Gritsun, A., Lykossov, V., Galin, V., Diansky, N., … Emelina, S. (2019d). *INM INM-CM5-0 model output prepared for CMIP6 CMIP historical.* Earth System Grid Federation. Retrieved from https://doi.org/10.22033/ESGF/CMIP6.5070 doi: 10.22033/ESGF/CMIP6.5070

Volodin, E., Mortikov, E., Gritsun, A., Lykossov, V., Galin, V., Diansky, N., … Emelina, S. (2019e). *INM INM-CM5-0 model output prepared for CMIP6 ScenarioMIP ssp126.* Earth System Grid Federation. Retrieved from https://doi.org/10.22033/ESGF/CMIP6.12326 doi: 10.22033/ESGF/CMIP6.12326

Volodin, E., Mortikov, E., Gritsun, A., Lykossov, V., Galin, V., Diansky, N., … Emelina, S. (2019f). *INM INM-CM5-0 model output prepared for CMIP6 ScenarioMIP ssp585.* Earth System Grid Federation. Retrieved from https://doi.org/10.22033/ESGF/CMIP6.12338 doi: 10.22033/ESGF/CMIP6.12338

Wieners, K.-H., Giorgetta, M., Jungclaus, J., Reick, C., Esch, M., Bittner, M., … Roeckner, E. (2019a). *MPI-M MPI-ESM1.2-LR model output prepared for CMIP6 CMIP historical.* Earth System Grid Federation. Retrieved from https://doi.org/10.22033/ESGF/CMIP6.6595 doi: 10.22033/ESGF/CMIP6.6595

Wieners, K.-H., Giorgetta, M., Jungclaus, J., Reick, C., Esch, M., Bittner, M., … Roeckner, E. (2019b). *MPI-M MPI-ESM1.2-LR model output prepared for CMIP6 ScenarioMIP ssp126.* Earth System Grid Federation. Retrieved from https://doi.org/10.22033/ESGF/CMIP6.6690 doi: 10.22033/ESGF/CMIP6.6690

Wieners, K.-H., Giorgetta, M., Jungclaus, J., Reick, C., Esch, M., Bittner, M., … Roeckner, E. (2019c). *MPI-M MPI-ESM1.2-LR model output prepared for CMIP6 ScenarioMIP ssp585.* Earth System Grid Federation. Retrieved from https://doi.org/10.22033/ESGF/CMIP6.6705 doi: 10.22033/ESGF/CMIP6.6705

Wu, T., Chu, M., Dong, M., Fang, Y., Jie, W., Li, J., … Zhang, Y. (2018). *BCC BCC-CSM2MR model output prepared for CMIP6 CMIP historical.* Earth System Grid Federation. Retrieved from https://doi.org/10.22033/ESGF/CMIP6.2948 doi: 10.22033/ESGF/CMIP6.2948

Xin, X., Wu, T., Shi, X., Zhang, F., Li, J., Chu, M., … Wei, M. (2019a). *BCC BCC-CSM2MR model output prepared for CMIP6 ScenarioMIP ssp126.* Earth System Grid Federation. Retrieved from https://doi.org/10.22033/ESGF/CMIP6.3028 doi: 10.22033/ESGF/CMIP6.3028

Xin, X., Wu, T., Shi, X., Zhang, F., Li, J., Chu, M., … Wei, M. (2019b). *BCC BCC-CSM2MR model output prepared for CMIP6 ScenarioMIP ssp585.* Earth System Grid Federation. Retrieved from https://doi.org/10.22033/ESGF/CMIP6.3050 doi: 10.22033/ESGF/CMIP6.3050

Yukimoto, S., Koshiro, T., Kawai, H., Oshima, N., Yoshida, K., Urakawa, S., … Adachi, Y. (2019a). *MRI MRI-ESM2.0 model output prepared for CMIP6 CMIP historical.* Earth System Grid Federation. Retrieved from https://doi.org/10.22033/ESGF/CMIP6.6842 doi: 10.22033/ESGF/CMIP6.6842

Yukimoto, S., Koshiro, T., Kawai, H., Oshima, N., Yoshida, K., Urakawa, S., … Adachi, Y. (2019b). *MRI MRI-ESM2.0 model output prepared for CMIP6 ScenarioMIP ssp126.* Earth System Grid Federation. Retrieved from https://doi.org/10.22033/ESGF/CMIP6.6909 doi: 10.22033/ESGF/CMIP6.6909

Yukimoto, S., Koshiro, T., Kawai, H., Oshima, N., Yoshida, K., Urakawa, S., … Adachi, Y. (2019c). *MRI MRI-ESM2.0 model output prepared for CMIP6 ScenarioMIP ssp585.* Earth System Grid Federation. Retrieved from https://doi.org/10.22033/ESGF/CMIP6.6929 doi: 10.22033/ESGF/CMIP6.6929

Figure 1. Cross-validation of annual river flow reconstruction and climate model simulations compared to observed river flows for the Po River at Pontelagoscuro from 1920 to 2012. (A) Reconstructed (REC) and observed (OBS) river flows, where grey and yellow shades represent the 95% prediction interval of the reconstructed series and the multiyear drought events derived from the observed river flows, respectively. (B) Kernel density profiles of river flows from observation, reconstruction, PMIP4 and CMIP6 simulations along with their respective mean values. Note that the CMIP6 mean (1,495 m^3/s) well captures the observed mean (1,497 m^3/s) thus these two lines are indistinguishable.

Figure 2. Annual river flow observation (OBS), reconstruction (REC), and simulations from PMIP4 and CMIP6 ensembles for the Po River at Pontelagoscuro from 1100 to 2100. (A) Time series of river flows. Reconstructed mean annual river flow during 1100–2012, colored by their departures from the reconstructed long-term mean (blue bars for positive, orange bars for negative, and grey shade for uncertainty range). Yellow and blue shades highlight drought periods identified with run theory applied to reconstructed data and the documented flood-rich periods, respectively. The light red shading shows the interquartile range for the 30-year moving average of the 25-model CMIP6 ensemble, encompassing both historical simulations (1850–2014) and future SSP5-8.5 projections (2015–2100). (B) Kernel density profiles of river flow observation (OBS), reconstruction (REC), and simulations from PMIP4 and CMIP6 ensembles across distinct periods: instrumental (1807–2023), paleo (1100–1849), historical (1850–2014), and future (2015–2100), along with their respective mean values.

Figure 3. Characteristics of past and future multiyear hydrological droughts for the Po River at Pontelagoscuro from 1100 to 2100. (A) Mean drought frequency (DF), duration (DD), severity (DS), and intensity (DD) for multiyear hydrological droughts exhibited by river flow observation (OBS), reconstruction (REC), and simulations from PMIP4 and CMIP6 across various periods, including the paleo period (1100–1849), historical epoch (1850–2014), and two prospective future scenarios (2015–2100). Solid lines represent the interquartile range. (B) Kernel density profiles of DD, DS, and DI of river flow observation (OBS), reconstruction (REC), and simulations from PMIP4 and CMIP6 across distinct periods.

Figure 4. Drought occurrence and cumulative drought deficit for the Po River at Pontelagoscuro from 1100 to 2100. Comparison between observed annual river flow (OBS) with (A) reconstruction (REC) and future projections from CMIP6 ensemble and (B) paleosimulations and future projections from PMIP4 ensemble. The yellow dashed line represents the lower band of the uncertainty range of reconstruction. The red and blue shade lines represent the full range of both CMIP6 and PMIP4 models for past simulations and future projections. (C) Comparison between 10-year moving average series of river flow observation (OBS), reconstruction (REC), PMIP4 ensemble, and CMIP6 ensemble. (D) Same as (C) but with a 30-year moving average which represents multidecadal dry periods. (E) Progression of the cumulative deficit from the drought onsets from observed and reconstructed multiyear drought events, where events with a shorter duration or smaller deficit than the 2015–2023 event are depicted in grey. (F) Same as (E) but paleosimulations from PMIP4 ensemble and future projections from CMIP6 ensemble under SSP5-8.5. The horizontal red dashed line represents the deficit of the most severe event in the paleo period.

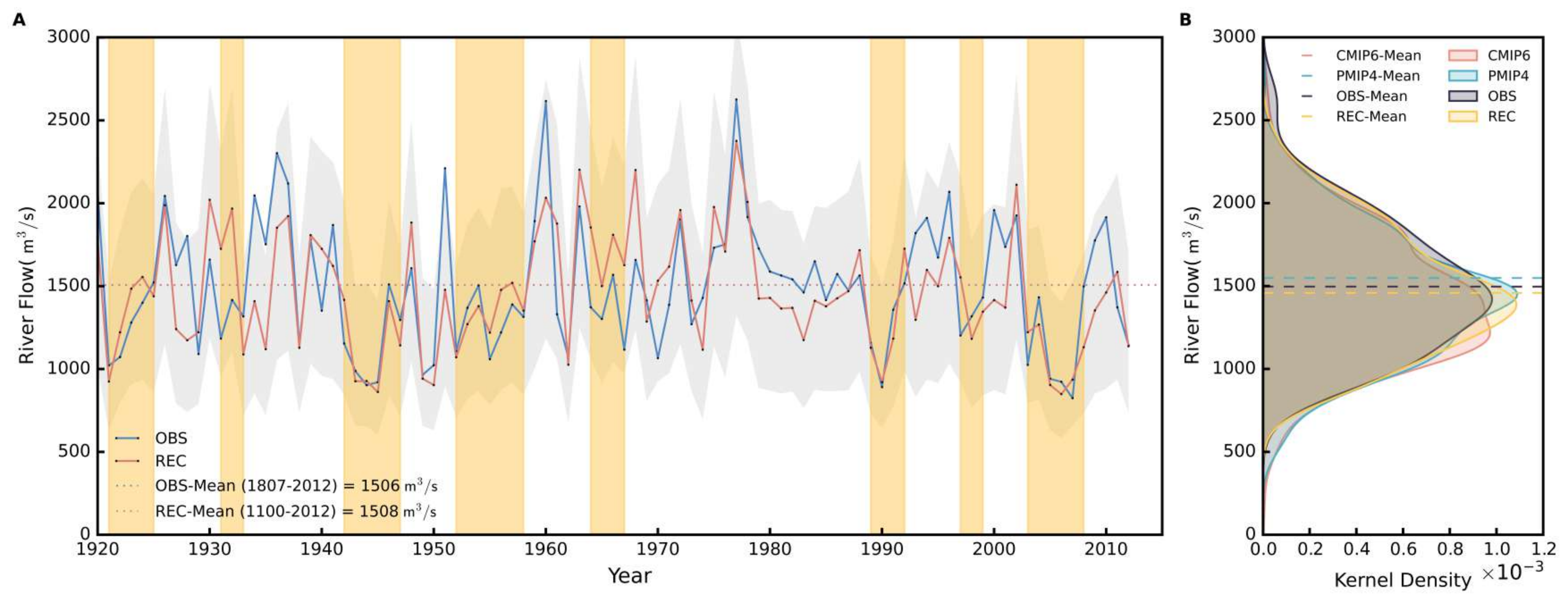

A
B
River Flow(m^3/s)
Year
OBS
REC
OBS-Mean (1807-2012) = 1506 m^3/s
REC-Mean (1100-2012) = 1508 m^3/s
CMIP6-Mean
PMIP4-Mean
OBS-Mean
REC-Mean
CMIP6
PMIP4
OBS
REC
Kernel Density $\times 10^{-3}$

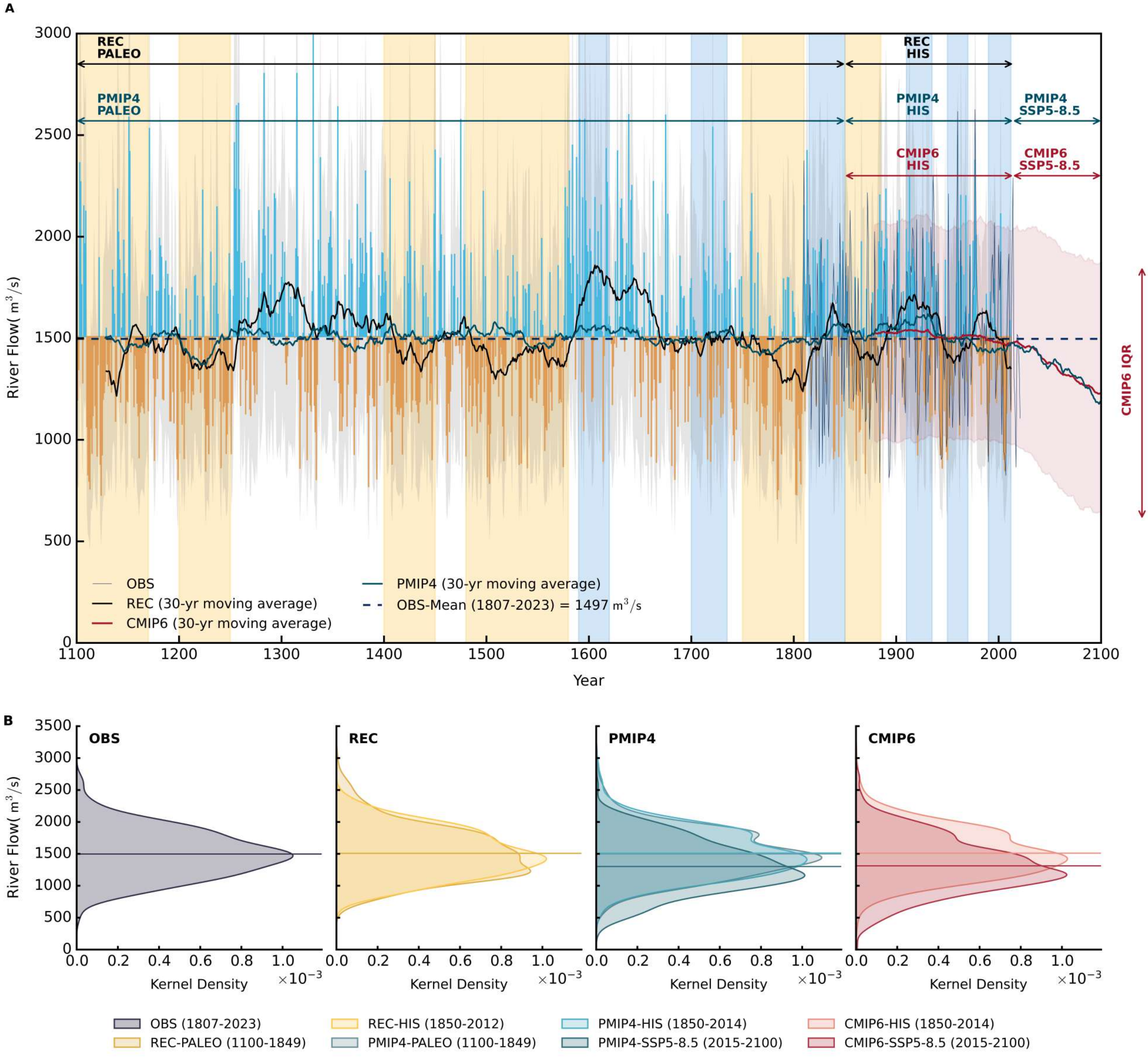
A
REC PALEO
REC HIS
PMIP4 PALEO
PMIP4 HIS
PMIP4 SSP5-8.5
CMIP6 HIS
CMIP6 SSP5-8.5
CMIP6 IQR
River Flow(m^3/s)
Year
OBS
REC (30-yr moving average)
CMIP6 (30-yr moving average)
PMIP4 (30-yr moving average)
OBS-Mean (1807-2023) = 1497 m^3/s
B
OBS
REC
PMIP4
CMIP6
Kernel Density
×10^{-3}
OBS (1807-2023)
REC-PALEO (1100-1849)
REC-HIS (1850-2012)
PMIP4-PALEO (1100-1849)
PMIP4-HIS (1850-2014)
PMIP4-SSP5-8.5 (2015-2100)
CMIP6-HIS (1850-2014)
CMIP6-SSP5-8.5 (2015-2100)

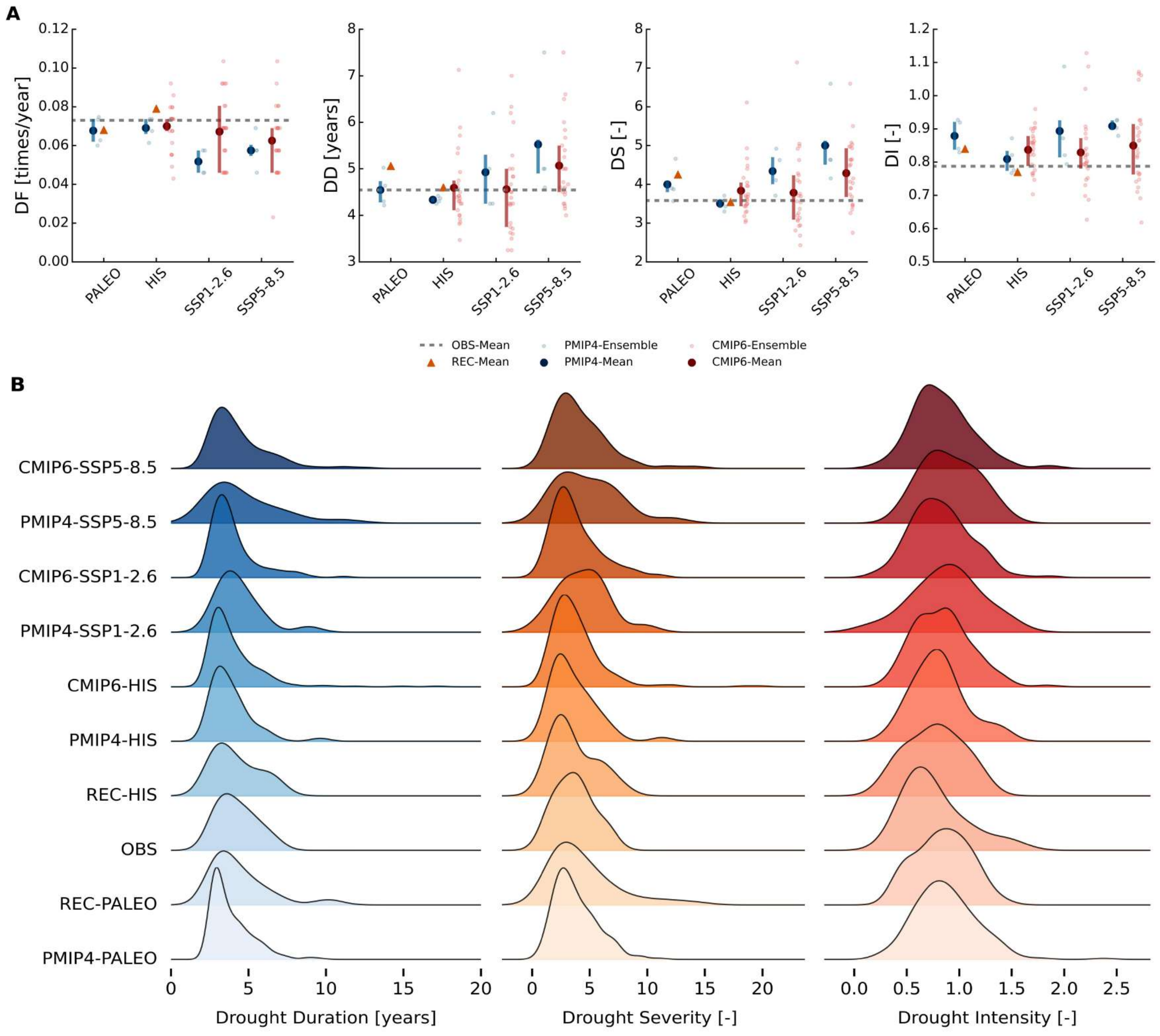
A
DF [times/year]
0.00
0.02
0.04
0.06
0.08
0.10
0.12
DD [years]
DS [-]
DI [-]
PALEO
HIS
SSP1-2.6
SSP5-8.5
OBS-Mean
REC-Mean
PMIP4-Ensemble
PMIP4-Mean
CMIP6-Ensemble
CMIP6-Mean
B
CMIP6-SSP5-8.5
PMIP4-SSP5-8.5
CMIP6-SSP1-2.6
PMIP4-SSP1-2.6
CMIP6-HIS
PMIP4-HIS
REC-HIS
OBS
REC-PALEO
PMIP4-PALEO
Drought Duration [years]
Drought Severity [-]
Drought Intensity [-]

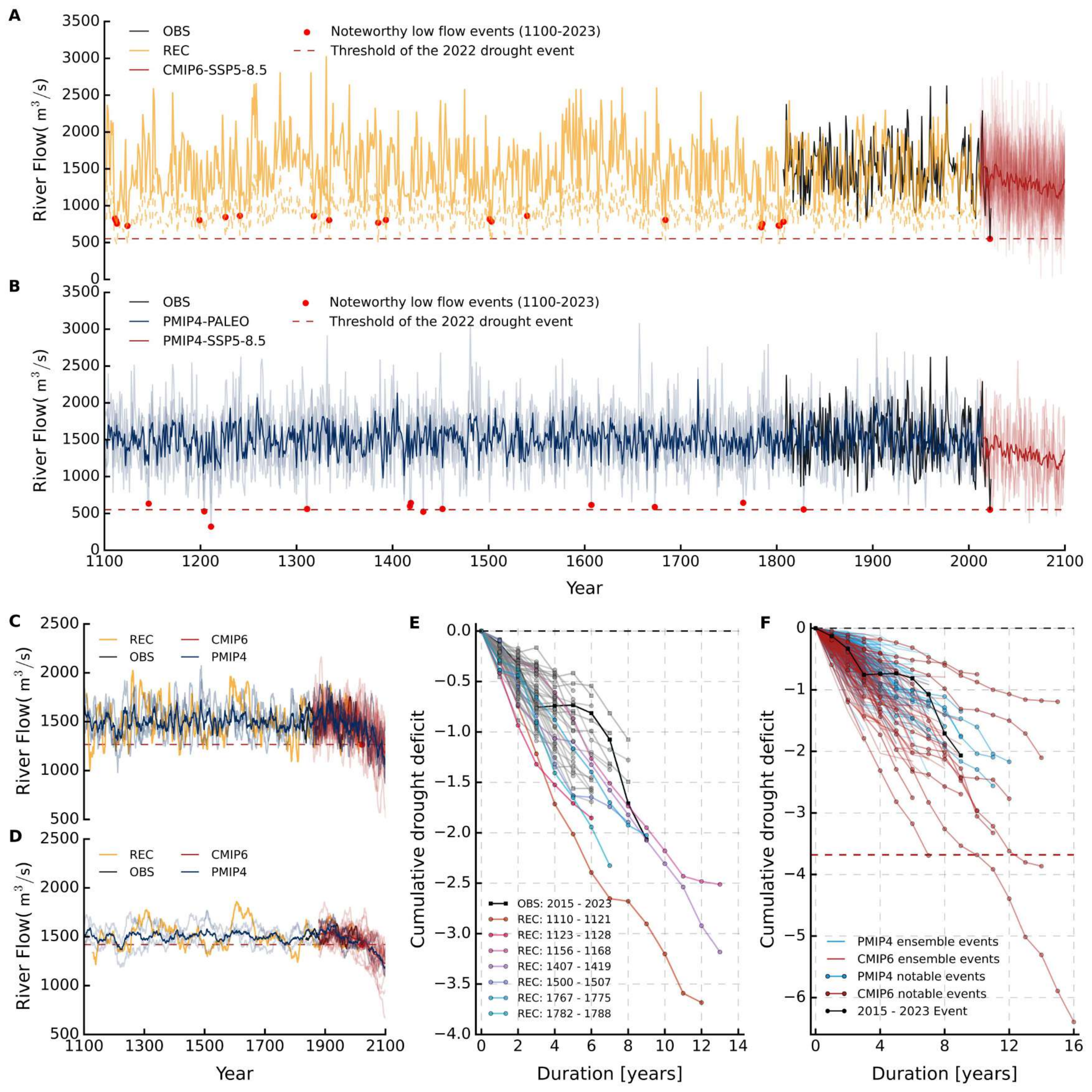

A
B
C
D
E
F
OBS
REC
CMIP6-SSP5-8.5
Noteworthy low flow events (1100-2023)
Threshold of the 2022 drought event
PMIP4-PALEO
PMIP4-SSP5-8.5
River Flow(m^3/s)
Year
CMIP6
PMIP4
Cumulative drought deficit
Duration [years]
OBS: 2015 - 2023
REC: 1110 - 1121
REC: 1123 - 1128
REC: 1156 - 1168
REC: 1407 - 1419
REC: 1500 - 1507
REC: 1767 - 1775
REC: 1782 - 1788
PMIP4 ensemble events
CMIP6 ensemble events
PMIP4 notable events
CMIP6 notable events
2015 - 2023 Event